

Tunable Josephson voltage source for quantum circuits

J.-L. Smirr,¹ P. Manset,¹ and Ç. Ö. Girit^{1,2,*}

¹JEIP, UAR 3573, CNRS, Collège de France, PSL University,
11, place Marcelin Berthelot, 75005 Paris, France

²Quantronics Group, Université Paris Saclay, CEA, CNRS, SPEC, 91191 Gif-sur-Yvette, France
(Dated: December 16, 2024)

Noisy voltage sources can be a limiting factor for fundamental physics experiments as well as for device applications in quantum information, mesoscopic circuits, magnetometry, and other fields. The best commercial DC voltage sources can be programmed to approximately six digits and have intrinsic noise in the microvolt range. On the other hand the noise level in metrological Josephson-junction based voltage standards is sub-femtovolt. Although such voltage standards can be considered “noiseless,” they are generally not designed for continuous tuning of the output voltage nor for supplying current to a load at cryogenic temperatures. We propose a Josephson effect based voltage source, as opposed to a voltage standard, operating in the 30–160 μV range which can supply over 100 nA of current to loads at mK temperatures. We describe the operating principle, the sample design, and the calibration procedure to obtain continuous tunability. We show current-voltage characteristics of the device, demonstrate how the voltage can be adjusted without DC control connections to room-temperature electronics, and showcase an experiment coupling the source to a mesoscopic load, a small Josephson junction. Finally we characterize the performance of our source by measuring the voltage noise at the load, 50 pV RMS, which is attributed to parasitic resistances in the cabling. This work establishes the use of the Josephson effect for voltage biasing extremely sensitive quantum devices.

Low-noise voltage sources are essential for sensitive electronics and basic science. The ultimate in voltage accuracy and precision are quantum voltage standards based on the Josephson effect [1]. The parts-per-billion frequency stability of microwave oscillators combined with the AC Josephson relation, $V = (2e/h) \cdot f$, between voltage V and frequency f , have enabled a metrological definition of the Volt [2]. Although Josephson standards are excellent for calibration or reference purposes [3], certain limitations have prevented their use as tunable voltage sources for precision applications in fields such as quantum information and mesoscopic physics. Most Josephson standards only provide a single fixed voltage between 1–10 V. The programmable Josephson voltage standard (PJVS) allows adjusting the reference voltage, but only in discrete steps with undefined transient voltages during changes [4]. The Josephson arbitrary waveform synthesizer (JAWS) allows fine voltage resolution but requires complicated pulse generation circuitry [5].

Here we demonstrate a tunable, very low-noise, metrologically accurate, voltage source [6] which can operate continuously in the range 30–160 μV and which is simple to implement as it only requires a tunable microwave generator. This voltage range is suitable for applications such as Josephson spectroscopy [7], topological transconductance quantization [8], dc-pumped parametric amplification and squeezing [9, 10], single microwave photon generation [11, 12], entangled beam generation [13, 14], and quantum thermodynamic engines [15].

The Josephson tunable voltage source is shown in Fig. 1. A Josephson junction of critical current I_c

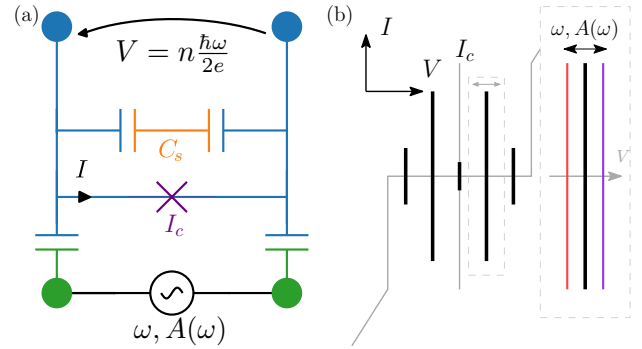


Figure 1. (a) Electrical circuit of a capacitively shunted Josephson junction (purple cross, critical current I_c) connected to a microwave source of frequency ω and amplitude $A(\omega)$. For A large enough, the junction current-voltage characteristic (b) shows vertical current spikes (Shapiro steps) at voltages $V = n\hbar\omega/2e$. By simultaneously adjusting ω and $A(\omega)$, the step voltage can be tuned while maintaining a large amplitude.

is capacitively coupled to a microwave voltage source of frequency ω and amplitude $A(\omega)$, Fig. 1(a). The junction is shunted by a capacitance C_s , which lowers the plasma frequency, ω_p , allowing stable operation at lower voltages [16]. A direct connection is used to source the DC voltage to another device or for characterization. The operation of the voltage source can be understood from a sketch of its current-voltage (IV) characteristic, Fig. 1(b). For appropriate values of microwave power, the IV characteristic shows vertical current peaks at voltages $V_n = n\hbar\omega/2e$, called Shapiro steps [17]. Biased on a Shapiro step of order n , the junction phase $\varphi \approx n\omega t$ is locked to the microwave drive and inherits its phase

* caglar.girit@cnrs.fr

stability. The junction acts as a noiseless voltage source which can supply currents close to the maximum of the peak, $I_n(V_n)$.

Although the step position depends solely on the microwave frequency and fundamental constants, the height of a Shapiro step depends on the microwave power at the junction, which varies with both the amplitude and frequency of the microwave source. When increasing the microwave power at fixed drive frequency, the Shapiro step heights will pass through successive maxima, separated by zeros where phase locking the voltage is not possible. Attenuation and imperfections in the transmission lines connecting the source to the junction, as well as the impedance mismatch at the junction, will influence the power delivered to the junction. In addition, due to the Josephson nonlinearity [18], the effective junction impedance depends strongly on frequency and drive amplitude for $\omega \lesssim \omega_p$. Because of the variability in coupled power with frequency, it is in general impossible to stay voltage locked while adjusting the drive frequency at constant drive amplitude. If the drive frequency falls on a value where the step height is zero, the voltage will switch to another step at different n , to the zero-current subgap region in between steps, or to the quasiparticle branch of the junction. However, after careful calibration one can adjust the microwave amplitude $A(\omega)$ simultaneously with ω in order to remain locked on a Shapiro step $V_n(\omega)$ over a wide range of frequencies, Fig. 1(b, right).

Images of the microfabricated device are shown in Fig. 2(a), where the junction, capacitors, and pads have been colored to match the schematic in Fig. 1(a). The device is loaded in a custom broadband microwave sample holder designed for operation up to 40 GHz and cooled in a dilution refrigerator with a base temperature below 10 mK. Electrical connections for DC source (blue) and AC drive (green) are made via wirebonds to the indicated pads. The DC measurement lines are filtered to reduce electronic noise and the microwave lines are attenuated to limit radiation from room temperature. Details of the experimental setup are found in Appendix A.

The Josephson tunnel junction is made of aluminum and has a gap voltage of $2\Delta/e = 400 \mu\text{V}$. Its current voltage characteristic is shown in Fig. 2(b). The mean switching current is 600 nA, close to the value of the current at the quasiparticle knee, as expected by the Ambegaokar-Baratoff theory [7]. The plasma frequency of the capacitively shunted junction is estimated to be $\omega_p = 6.8 \text{ GHz}$. This value is deduced from comparing the geometry, fabrication parameters and measured critical currents to two similar samples where ω_p was determined as the frequency at which the junction IV characteristic is most sensitive to microwave drive. At resonant drive, $\omega \approx \omega_p$, the IV is strongly distorted even at extremely small power levels.

The shunt capacitor is a metal-insulator-metal structure with aluminum oxide dielectric and aluminum pads deposited by electron-beam evaporation. From the measured value of I_c and ω_p , and ignoring the intrinsic junc-

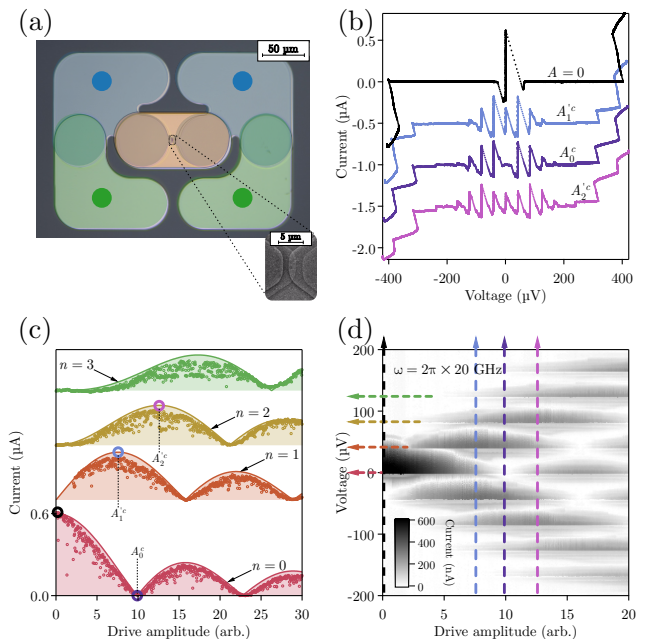


Figure 2. (a) False-colored optical image of device and micrograph of the junction (purple cross, inset). Colors of bonding pads (green, blue) and shunt capacitor (orange) correspond to schematic Fig. 1(a). (b) Current-voltage characteristics of device without (black) and with microwave drive at $\omega = 2\pi \times 20 \text{ GHz}$ and three different power levels (traces offset by $0.5 \mu\text{A}$). (c) The height of the supercurrent peak and first three Shapiro steps are extracted from the current-voltage map (d) and plotted as a function of microwave power.

tion capacitance, we determine that $C_s \approx 2eI_c/\hbar\omega_p^2 = 1.35 \text{ pF}$, which is consistent with the dimensions and dielectric constant.

In the absence of microwave drive, $A = 0$, the measured current-voltage characteristic, Fig. 2(b), shows a single peak at zero voltage, the supercurrent peak (black trace). Shapiro steps appear when the junction is driven with microwaves at frequency $\omega_0/2\pi = 20 \text{ GHz}$ (blue). At an appropriate microwave drive strength, corresponding to a critical amplitude A_1^c , the height of the first order peak at $V = \hbar\omega_0/2e = 41.4 \mu\text{V}$ is maximal and approximately 250 nA. Increasing the microwave amplitude to $A(\omega_0) = A_0^c$, the supercurrent peak ($n = 0$) vanishes but steps of higher order persist. With stronger microwave drive steps of higher order can be maximized, such as the second one (A_2^c). In this notation, at drive amplitude A_n^c the n -th current peak is at a maximum, whereas at A_n^c the n -th peak is at its first non-trivial zero.

In Fig. 2(d), the IV characteristics are plotted as a 2D map over a broad range of microwave power, with each pixel corresponding to the maximal absolute value of the measured current at a given bias voltage and drive amplitude. Shapiro steps appear as dark gray points grouped in horizontal line segments, with the contrast indicating the step height. The periodic, triangular pattern is expected from the Bessel function dependence of step

heights [16]. The IV traces of Fig. 2(b), measured at constant power, are indicated by vertical dashed lines.

The height of steps $n = 0 - 3$, determined by taking the corresponding cuts of Fig. 2(d) (horizontal dashed arrows), are plotted as a function of microwave power in Fig. 2(c). They are fit to Bessel functions of the first kind, $|J_n|$, for orders $n = 0 - 3$. In contrast to Fig. 2(b), here we see the continuous evolution of the step heights with $A(\omega)$: the supercurrent peak decreases and reaches its first zero (A_0^c) while the first- and second-order peaks reach their respective maxima at A_1^c and A_2^c .

In principle any of the critical points $A_0^c(\omega), A_1^c(\omega)$, or $A_2^c(\omega)$ can be used to calibrate the incident power at the junction for frequencies $\omega \gtrsim \omega_p$, where the Bessel function dependence is valid. Junctions biased at lobe maxima, such as $A_1^c(\omega)$ and $A_2^c(\omega)$, serve as square law power detectors whereas junctions at Bessel function zeros such as $A_0^c(\omega)$ are linear detectors [19, 20]. In addition to calibrating the microwave power using the Josephson effect, photon-assisted tunneling (PAT) of quasiparticles near the gap voltage can also serve for calibration [21].

For simplicity we either use the first zero of the supercurrent, $A_0^c(\omega)$, or the PAT current to calibrate the power for a frequency range spanning approximately 8–40 GHz. Both of these techniques avoid complications arising from the hysteretic, non-linear shape of the junction IV characteristic. At each frequency we determine the power necessary to either zero the supercurrent or to obtain a reference value of the PAT current near the quasiparticle knee. From the Bessel function dependence of the critical point or the PAT current, we calculate the drive power necessary to maximize the Shapiro step of a given order. Technical details of the calibration procedure are given in Appendix B.

In order to demonstrate the quality of the calibration, Fig. 3(a) plots current-voltage characteristics with a microwave drive at 16 GHz, 18 GHz and 20 GHz and amplitudes $A_0^c(\omega)$ corresponding to the first zero of the supercurrent. Shapiro steps up to order $n = 4$ are visible at multiples of voltages $33.09 \mu\text{V}$ for 16 GHz drive, $37.22 \mu\text{V}$ (18 GHz), and $41.36 \mu\text{V}$ (20 GHz), with a corresponding step spacing $n \cdot 2 \text{ GHz} \cdot h/2e \approx n \cdot 4.14 \text{ uV}$. As anticipated in the schematic, Fig. 1(b), the Shapiro step height within each order is approximately the same. A figure of merit μ for calibration is the ratio of the residual mean switching current, which should be zero for perfect calibration, to the maximum switching current, which is approximately 600 nA in the reference IV without microwave drive (black trace). The residual mean switching current for all three frequencies in Fig. 3(a) is less than 20 nA, giving $\mu \approx 3\%$.

Fig. 3(b) shows a current-voltage map when driving at amplitude $A_0^c(\omega)$ over a wide frequency range. Measured average voltage is on the left axis, applied microwave drive frequency is on the bottom axis, and the maximum absolute value of the measured current is represented by the pixel contrast. The IV s of Fig. 3(a) at 16 GHz, 18 GHz and 20 GHz are indicated by color-coded

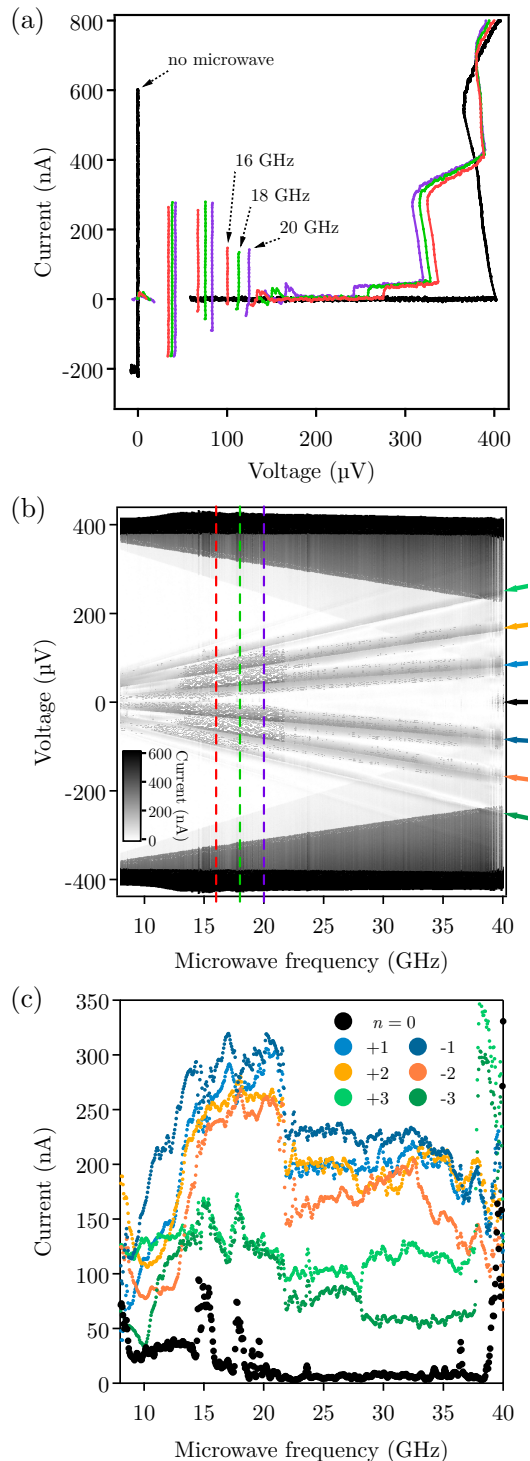


Figure 3. (a) Current voltage characteristics measured at optimal microwave amplitude $A_0^c(\omega)$ minimizing the supercurrent for $\omega/2\pi = 16$ GHz, 18 GHz and 20 GHz. A reference IV without microwave drive is shown in black. Data measured with a positive sweep in bias voltage, resulting in smaller negative peaks. (b) Current voltage map measured at $A_0^c(\omega)$ plotted as a function of microwave drive frequency. The IV characteristics in (a) are indicated by vertical dashed lines. (c) Height of Shapiro peaks of order n extracted from (b) along the lines indicated by arrows.

dashed vertical lines. Colored arrows along the right axis indicate Shapiro steps of order $n = -3$ to $n = 3$. Since the microwave drive is adjusted to $A_0^c(\omega)$, the supercurrent peak along the horizontal axis is virtually absent, and the non-zero orders are well visible although none is maximized.

From the current voltage map we numerically extract the mean switching current of the Shapiro steps and plot them as a function of frequency, Fig. 3(c). The residual supercurrent (black trace) is low, with $\mu \lesssim 10\%$ for almost the entire frequency range. In addition, the height of the first order steps ($n = \pm 1$, blue traces) is more than 200 nA, or approximately a third of the zero-drive supercurrent, for a large range of frequencies. The Bessel function dependence of step heights predicts that the first order steps should be approximately 0.519 times the supercurrent peak for a microwave drive $A_0^c(\omega)$, and this appears to be the case in the frequency range 15–20 GHz, where the peak height reaches 300 nA. The measured step heights for the higher orders also agrees with theory, as the expected peak height ratios I_n/I_c for $n = 2, 3$ are 0.432 and 0.2, respectively, compared to $1/3$ ($n = \pm 2$, orange traces) and $1/6$ ($n = \pm 3$, green traces) estimated from the data.

Some of the measured variation of peak heights in Fig. 3(c) can be explained, such as the sharp drop above approximately 22 GHz which is attributed to the deactivation of an attenuator resulting in increased power fluctuations and lower switching currents. Discrepancies at lower frequencies may be due to weaker applicability of the Bessel function form for step heights in that frequency range. Furthermore, microwave resonances on chip or in the sample box may give rise to the narrow features superposed on a generally smooth step height dependence.

To use the device as a tunable voltage source it is crucial that the step height amplitudes do not dip towards zero in the entire frequency range. Such dips will reduce the maximum possible source current and in the worst case, destroy phase lock. A load that sinks current larger than the step amplitude will cause the source to switch off the Shapiro step. With our calibration procedure it is possible to source at least 50 nA using any order over almost the entire frequency range, with the only exception a narrow region near 10 GHz at $n = -3$.

Next we consider the possibility of voltage locking without DC bias. Shapiro steps which cross at zero current, as shown in the sketch Fig. 1(b) and demonstrated in the IV characteristic Fig. 3(a), may occur in underdamped Josephson junctions [22] and are used in zero-bias voltage standards [16, 23]. A non-zero voltage locked state is stable even in the absence of a bias current, and a voltage $n\hbar\omega/2e$ for $n > 1$ can spontaneously develop across a microwave driven junction.

In Fig. 4, we show how the DC voltage on our junction can spontaneously lock to the drive frequency without any DC bias and then remain locked as the voltage is tuned continuously over a large range. In the

circuit shown in the inset, the DC current bias leads have been disconnected with a cryogenic switch (KEMET EC2-12SNU) [24]. However the junction voltage V can still be measured with DC connections to a voltage amplifier with high input impedance and negligible input bias current (NF LI-75A). In order to spontaneously switch to a Shapiro step, the phase must first unlock from the supercurrent branch at $n = 0$. To do so the amplitude is ramped to the calibration point $A_0^c(\omega)$ where the effective supercurrent is zero. At this point, as a result of fluctuations, the voltage jumps to a Shapiro step of positive or negative polarity. We then set the power to maximize the step height according to the calibration value $A_n^c(\omega)$, subsequently adjusting it in tandem with the frequency.

Over a period of 100 min ($n = 1$) or about 9 s ($n = 2$), we ramp the frequency up and down while locked to the first or second order Shapiro step. The curve is continuous, and the voltage does not switch to zero or to another step.

To use the Josephson source in an experiment requiring a noiseless, tunable DC voltage, the device under test (DUT) should be connected to the source via a low resistance, high inductance interconnect, as shown in the circuit Fig. 5(a). Any parasitic resistance r_p between source and DUT should be as small as possible in order to limit thermal noise. The inductance L serves as an RF choke, blocking the microwave drive at ω_0 as well as harmonics $n\omega_0$ generated by the source. Ideally the interconnection between source and DUT should be designed to avoid resonances at frequencies in the desired voltage range. The source and DUT can be located in the same enclosure, taking care to avoid microwave leakage between the source and DUT compartments, or in separate sample boxes.

As a proof-of-concept demonstration, we connect the source to a DUT which is itself a small Josephson tunnel junction of critical current $I_e \approx 140$ nA $\approx I_c/6$ Fig. 5(a, small purple cross). Source and emitter are located in separate enclosures and connected by a superconducting twisted pair cable Fig. 6. Due to the AC Josephson effect this “emitter” DUT converts the DC voltage from the source to a microwave signal. Since the measured linewidth is proportional to the DC voltage noise at the emitter, we can characterize the residual voltage noise of our setup. The Josephson emission linewidth has been directly measured in this fashion for both large [25] and small junctions [26, 27] biased with a conventional, noisy, DC voltage source. Effectively the source junction downconverts a microwave drive to a DC voltage, which is then transmitted via low-frequency wiring to the emitter junction, which then upconverts the DC back to a microwave signal. We capacitively couple the emitter to a cryogenic amplifier and measure the linewidth with a microwave spectrum analyzer.

The microwave drive frequency is $\omega_0/2\pi = 7.69$ GHz and the amplitude has been chosen to maximize the step of order $n = 2$. The source junction is DC biased on the second Shapiro step at $V_2 = 2\hbar\omega_0/2e$. This allows

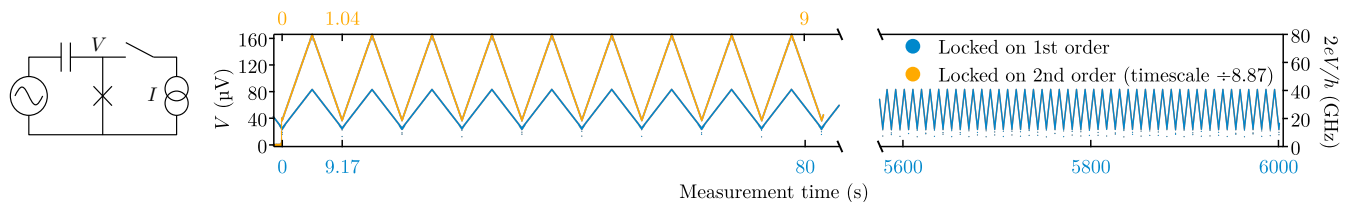


Figure 4. After switching to the first Shapiro step (blue) while the biasing circuit is disconnected (left), the frequency is modulated between 10–40 GHz with a triangular waveform with a period of 9.17 s. The power is adjusted according to the calibration to maintain the step amplitude. The measured junction voltage is continuous and follows the Josephson relation $V = \hbar\omega/2e$ without switching to other steps over a total time of 100 min. In orange the junction is locked to the second order step at $V = 2\hbar\omega/2e$, the sweep period is 1.036 s, and the measurement duration is approximately 9 sec.

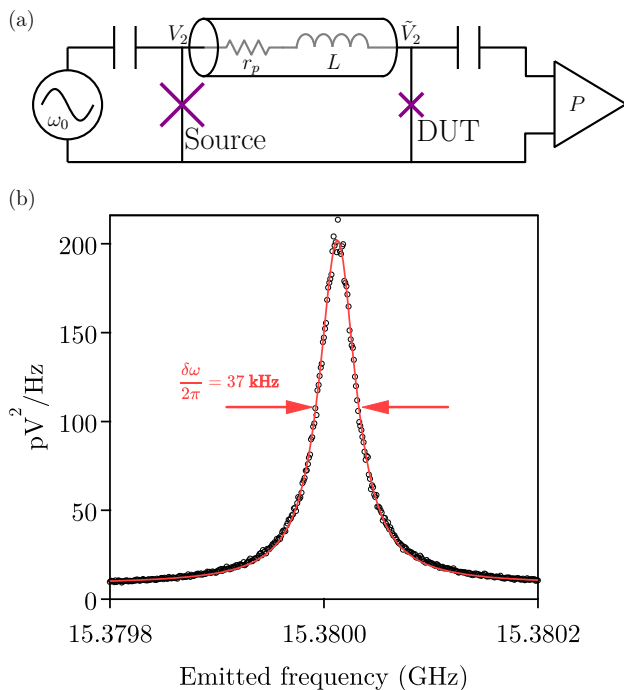


Figure 5. (a) A small Josephson junction (purple cross, right), serving as a device under test (DUT), is coupled to the Josephson voltage source (purple cross, left) via a superconducting twisted pair cable of inductance L and small parasitic resistance r_p . The source and DUT are located in separate sample boxes (Fig. 6). A microwave drive of frequency $\omega_0/2\pi = 7.690$ GHz is applied to switch the junction to the second Shapiro step at voltage $V_2 = 2\hbar\omega_0/2e = 31.80$ μ V. The DC voltage at the DUT, $\tilde{V}_2 \approx V_2$, is converted by the Josephson effect to a microwave signal of frequency $\omega_m \approx 2\omega_0$ which is measured with a microwave amplifier. (b) The power spectrum shows a narrow peak at $\omega_m/2\pi = 15.380\,012\,60(2)$ GHz with a FWHM linewidth of 37 kHz (red fit).

differentiating the emitter Josephson frequency $2\omega_0$ from the drive frequency ω_0 of the source junction. Although the second harmonic of the microwave drive generated by the Josephson non-linearity of the source junction is also at $2\omega_0 = 15.38$ GHz, it is heavily attenuated by the cable connecting the source to emitter. This ensures that we

measure the microwave signal resulting from downconversion to DC and subsequent upconversion by the emitter instead of direct frequency doubling by the source. We confirm there is no harmonic leakage by checking that the microwave power output of the emitter at $2\omega_0$ is independent of the power incident on the source junction, as long as the source junction is locked on the second Shapiro step. A direct frequency doubling process by the source junction would yield a Bessel function dependence of the power detected at $2\omega_0$, whereas upconversion from DC by the emitter yields a microwave current of amplitude bounded by I_e , independent of the incident power.

Fig. 5(b) shows the spectrum measured at the cryostat base temperature of approximately 7 mK. The full-width at half maximum (FWHM) of the Lorentzian peak is 37 kHz. The linewidth broadening, relative to that of the microwave source, can be explained by a small resistance r_p between source and emitter, indicated in the schematic Fig. 5(a). The peak position $\omega_m/2\pi = 15.380\,012\,60(2)$ GHz is detuned from $2\omega_0$ by a $\Delta\omega = 2\omega_0 - \omega_m \approx 2\pi \times 12.6$ kHz. This detuning can result from a parasitic DC current i_p flowing through the resistance r_p which gives a voltage drop $i_p r_p = \hbar\Delta\omega/2e = V_2 - \tilde{V}_2$. The origin of this DC current is likely to be inelastic Cooper pair tunneling [28, 29], in which the microwave power generated by the emitter and absorbed in its environment is balanced by the DC power supplied by the source.

We obtain $r_p \approx 20$ – 30 m Ω with three different methods: equating r_p with the known contact resistance of the connectors (30 m Ω); using $r_p = \hbar\Delta\omega/2ei_p$ with i_p estimated as the inelastic Cooper pair current arising from a 50 Ω microwave environment (20 m Ω); extracting r_p from the slope of the detuned voltage \tilde{V}_2 as a function of a current bias applied to the source (24 m Ω).

With zero series resistance between source and emitter, we would expect a much narrower linewidth than the measured value, 37 kHz. The emission linewidth is broadened by thermal fluctuations in the resistor r_p , which have a voltage noise density $4k_b T r_p$ where k_b is Boltzmann's constant and T is the electronic temperature. For a Lorentzian lineshape, the expected FWHM is $4\pi k_b T r_p (2e/h)^2$, assuming a rectangular power spec-

trum for the noise [26, 30]. This result is independent of the cutoff frequency, which could be thermal, $k_b T/h$, or given by $1/r_p C$ for sufficiently large $r_p C$, where C is the effective capacitance of the cables and wiring in parallel with the emitter junction.

Using $r_p = 25 \text{ m}\Omega$, the emission linewidth is compatible with a reasonable electronic temperature, $T = 36 \text{ mK}$. Reducing the linewidth to sub-kHz levels would require careful care to eliminate parasitic resistance between source and DUT. Every milliohm of resistance at a low electronic temperature of 25 mK contributes 1 kHz to the linewidth. When source and DUT are separated by superconducting wires, the resistance of connector pins, which dominates in this case, as well as solder and printed circuit trace resistances must be minimized. Despite the inadvertent parasitic resistance, the measured frequency precision is 2.4 ppm. The inferred low-frequency voltage noise density at the emitter junction is approximately $220 \text{ fV}/\sqrt{\text{Hz}}$, and the total RMS voltage noise is less than 50 pV.

We have demonstrated a tunable, low noise voltage source based on the AC Josephson effect, operating in the range 30–160 μV . The calibration procedure optimizes stability of the voltage output across a wide frequency range, and the source maintains phase lock without an applied DC bias for an indefinite period. One can connect to the voltage source with low-frequency superconducting wires or interconnects, taking care to minimize parasitic resistances, but it is not necessary to have source and load in the same enclosure. In practice, the DC connection to monitor the output voltage can be eliminated given the metrological relationship of source voltage to microwave drive frequency. In addition to continuous tunability, the source has low noise and metrological accuracy. Future work could explore extending the voltage range, possibly by using series arrays of Josephson junctions or employing different junction materials such as niobium, in conjunction with more complex microwave drive, such as biharmonic or pulsed, enabling deterministic switching to higher-order Shapiro steps. The current range could also be extended using larger junctions or parallel arrays. Improvements on microwave coupling efficiency could help reaching stability at voltages closer to zero. Our proof-of-concept experiment coupling the source to a small Josephson junction demonstrates the possibility of integrating ultra low-noise, tunable, cryogenic DC voltage bias into devices for quantum information, quantum sensing, and mesoscopic physics. Specific applications include microwave photon emitters [13, 26], Josephson spectroscopy [7, 31], dc-pumped parametric amplification [10, 32, 33], and qubit stabilization [34].

ACKNOWLEDGMENTS

We thank V. Benzoni, J. Griesmar, L. Peyruchat, J.-D. Pillet, and F. Lafont for discussions and assistance with the experiment. We thank Fabien Portier and Ambroise

Peugeot for critical feedback. This project has received funding from the European Research Council (ERC) under the European Union’s Horizon 2020 research and innovation programme (grant agreement 636744). The research was also supported by IDEX Grant No. ANR-10-IDEX-0001-02 PSL, a Paris “Programme Emergence(s)” Grant and the CNRS “Prématuration” programme.

Appendix A: Experimental Details

The experiments were conducted in a Bluefors LD250 dilution refrigerator with a base temperature below 10 mK. A photograph and a complete simplified circuit can be found in Fig. 6(a). The source IV characteristics are obtained by sweeping V_b with switch Sw closed. The voltage V is measured while the current I is calculated using $I = (V - V_b)/R$, where $R = 80 \Omega$ is the sum of two series thin film resistors. Thermal and instrument noise is filtered as shown in Fig. 7, where colors match that of Fig. 6(b).

All connections are made with balanced, differential twisted pairs. The 20Ω bias resistor r has a large volume in order to thermalize electrons. A room-temperature floating voltage source supplies a voltage V_0 which is attenuated ($\sim 1/25000$) and RC -filtered to produce the bias voltage V_b . Both V_b and V are measured by low-noise differential preamplifiers (NF LI-75). The DPDT electro-mechanical switch Sw (KEMET EC2-12SNU) is toggled by a $\pm 0.3 \text{ V}$, 0.1 s long pulse delivered via a superconducting twisted pair.

Bias, source and emitter are interconnected by NbTi twisted pairs about 30 cm long, providing inductance to attenuate high-frequencies while having zero DC resistance. The residual parasitic resistance r_p discussed in the main text is attributed to the pins of the connectors in the cable between source and DUT (LEMO 0.5 mm pins).

On the AC end of the source, the microwave drive is applied via coaxial cables with distributed attenuators totaling 23 dB. The 2–40 GHz hybrid coupler adds 3 dB attenuation but terminates the sample with a 50Ω load at 10 mK while dumping low-frequency noise to another 50Ω load.

On the AC end of the emitter, the spectrum is measured with a signal analyzer (Rohde&Schwarz FSVA30) after cryogenic (LNF LNC4_16C) and room-temperature (Mini-Circuits ZVA-183-S+) amplification. Two “0 dB” XMA attenuators help with cable thermalization. No other filtering is used.

The sample is mounted on a PCB covered by a copper lid used as a mechanical and thermal anchor to the mixing chamber of the cryostat, Fig. 8. To minimize the effect of electromagnetic cavity resonances, the sample box is designed to be small and Eccosorb absorber is affixed to the lid. The sample is magnetically shielded by the combination of an inner aluminum cylinder and an outer cylinder made of Cryophy, a high magnetic per-

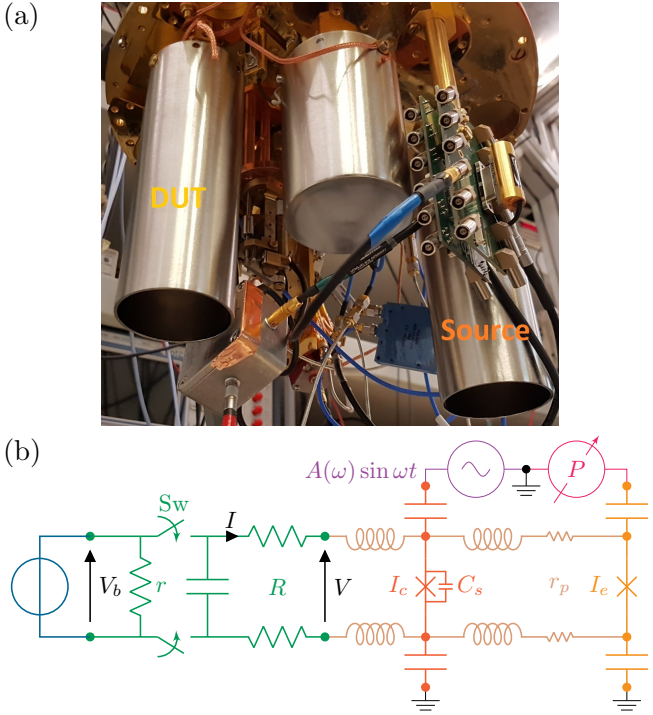


Figure 6. (a) Photo of the source (right) and emitter (left) in their magnetically-shielded sample holders attached to the dilution refrigerator. Source, emitter, and a biasing circuit box (not visible) are connected to each other by NbTi twisted pairs terminated by LEMO.00.302 connectors (not visible). Some elements appear on the photo which are not related to the experiment described in this article. (b) Schematic of the source (orange) connected to the emitter (gold) with biasing circuit (green) and source (blue) via NbTi twisted pairs (brown).

meability material compatible with low temperatures. The PCB includes sockets for a differential DC connector (LEMO 00.302) and a microwave connector (2.92mm).

The Dolan-type aluminum Josephson junction, shunt capacitor, and microwave coupling capacitor are fabricated using optical lithography and electron-beam evaporation. The bottom electrodes of the capacitors are deposited in the same step as the junction, followed by alumina evaporation constituting the first 30 nm of the insulators. The rest of the alumina insulation (60 nm) and the top electrodes (aluminum, 200 nm) are deposited after a second round of lithography. Electrical connection to the junction at the bottom electrode level is made via wirebonds which break through the insulating layers.

Appendix B: Calibration

In the article we discuss two methods for calibrating microwave power, i.e. obtaining values $A_n^c(\omega)$ of the drive amplitude that maximize a given n -th order Shapiro step at different frequencies. Calibrating at discrete values ω_i separated by 10 to 100 MHz is sufficient, and in-

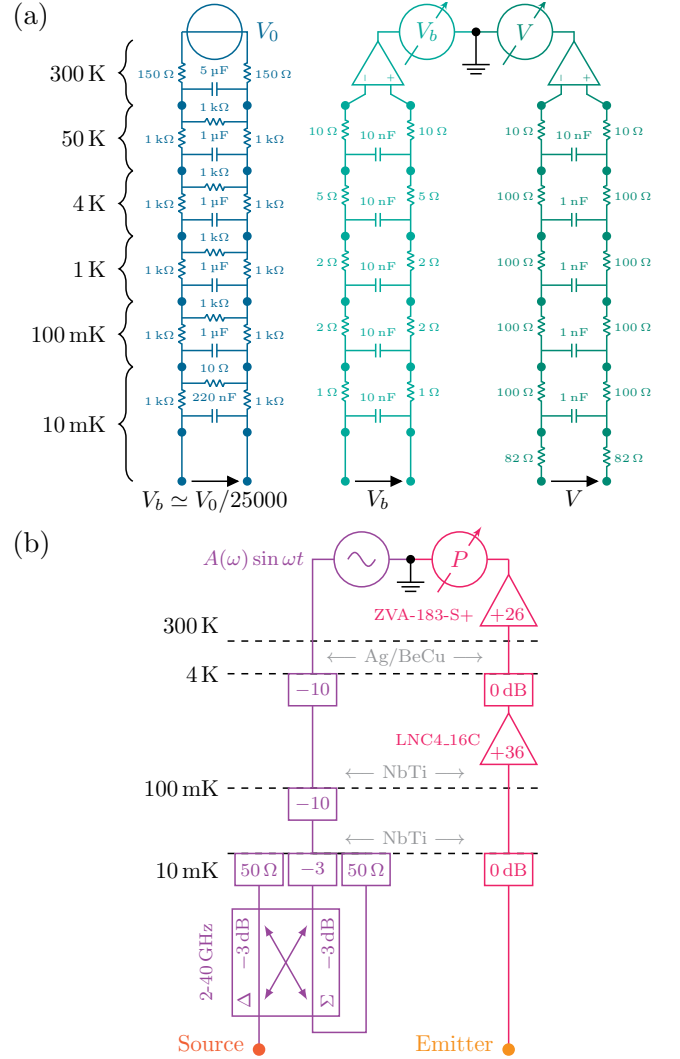


Figure 7. Details of the cryostat wiring: (a) DC wiring is made of twisted pairs equipped with filtering RC circuits thermally anchored at all temperature stages of the cryostat. (b) AC wiring uses standard copper coaxial cables with 2.92mm connectors except where specified: NbTi between 10 mK and 4 K, silver-plated BeCu from 4 K to room temperature. 1 K and 50 K stages are bypassed in AC.

intermediate frequencies can be obtained by interpolation.

The photon-assisted tunneling (PAT) method consists in choosing a reference PAT current I^* and finding the microwave drive amplitude $A^*(\omega_i)$ at which this PAT current is obtained for a given frequency ω_i . In practice, we bias the junction around a voltage V just below the superconducting gap, set a microwave frequency ω_i and amplitude A , which we modulate at a low rate f (typically 10–100 Hz). Then we proceed to a lock-in measurement of current I at frequency f . This enables measuring very low PAT currents where $I \propto A$. With such a linear relationship, it is straightforward to implement a software feedback loop that converges to the

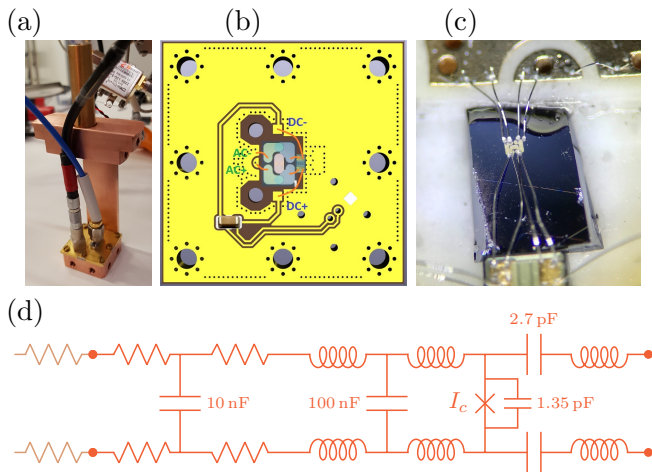


Figure 8. (a) Photo of the sample holder used for both source and emitter. Sample holders are housed in cylindrical shields visible in Fig. 6(a) (b) Drawing of the PCB and wirebonds to the source sample, indicating shunt capacitors. (c) Close-up photo of the sample wirebonded to the 2.92mm PCB launch and shunt capacitor. Wirebonds to DC pads are partially visible. (d) Electrical schematic of the source chip and PCB. Emitter schematic is identical, but the 1.35 pF on-chip shunt capacitor C_s is absent. Inductors represent Al wirebonds and resistors represent the non-superconducting elements, including cable connector (brown), socket and PCB tracks, which comprise the parasitic resistance r_p . Shunt capacitors reduce voltage noise.

value A^* corresponding to the reference PAT current I^* . Calibration data $A_n^c(\omega_i)$ is obtained by correcting values $A^*(\omega_i)$ by a constant factor that depends on chosen step n and reference PAT current I^* . A limitation of this method is that V should be adjusted with ω since the PAT current has a stepped distribution that shifts with drive frequency. Also it is difficult to reliably set V at lower drive frequencies because of the hysteresis in the IV characteristic near the superconducting gap. However, because PAT current is monotonic with A , it is a reliable method for moderate-accuracy calibration.

A more accurate calibration method uses the suppression of the supercurrent I_0 with drive power. The approximate position of the first zero of $I_0 = I_c J_0(A)$ is determined using the PAT calibration method. For each drive frequency ω_i , the amplitude A is swept around the position of the predicted zero. We record the amplitude $A_0^c(\omega_i)$ at which the junction switches to non-zero voltage. This constitutes the calibrated reference from which, using the properties of Bessel functions, we calculate $A_n^c(\omega_i)$, the amplitude that maximizes the Shapiro peak of order n . Experimentally, the supercurrent suppression is detected by measuring V while applying (via V_b) a small bias current $I = I_b \ll I_c$: when supercurrent is reduced to $I_0 \lesssim I_b$, the junction switches from zero-voltage to a finite voltage RI_b . I_b is chosen as small as permitted by the signal-to-noise ratio of V .

-
- [1] B. Jeanneret and S. P. Benz, *The European Physical Journal Special Topics* **172**, 181 (2009).
- [2] P. J. Mohr and B. N. Taylor, *Rev. Mod. Phys.* **77**, 107 (2002).
- [3] A. Rufenacht, N. E. Flowers-Jacobs, and S. P. Benz, *Metrologia* **55**, S152 (2018).
- [4] C. J. Burroughs, P. D. Dresselhaus, A. Rufenacht, D. Olaya, M. M. Elsbury, Y.-H. Tang, and S. P. Benz, *IEEE Transactions on Instrumentation and Measurement* **60**, 2482 (2011).
- [5] S. P. Benz and C. A. Hamilton, *Applied Physics Letters* **68**, 3171 (1996).
- [6] C. Girit and J.-L. Smirr, Voltage source and method for calibrating this voltage source (2023), FR patent FR3114171B1, US patent US20230341880A1 pend.
- [7] J. Griesmar, R. H. Rodriguez, V. Benzoni, J.-D. Pillet, J.-L. Smirr, F. Lafont, and Ç. Ö. Girit, *Physical Review Research* **3**, 043078 (2021), publisher: American Physical Society.
- [8] L. Peyruchat, J. Griesmar, J.-D. Pillet, and Ç. Ö. Girit, *Physical Review Research* **3**, 013289 (2021), publisher: American Physical Society.
- [9] S. Jebari, F. Blanchet, A. Grimm, D. Hazra, R. Albert, P. Joyez, D. Vion, D. Estève, F. Portier, and M. Hofheinz, *Nature Electronics* **1**, 223 (2018).
- [10] U. C. Mendes, S. Jezouin, P. Joyez, B. Reulet, A. Blais, F. Portier, C. Mora, and C. Altimiras, *Physical Review Applied* **11**, 034035 (2019), publisher: American Physical Society.
- [11] A. Grimm, F. Blanchet, R. Albert, J. Leppäkangas, S. Jebari, D. Hazra, F. Gustavo, J.-L. Thomassin, E. Dupont-Ferrier, F. Portier, and M. Hofheinz, *Physical Review X* **9**, 021016 (2019).
- [12] C. Rolland, A. Peugeot, S. Dambach, M. Westig, B. Kubala, Y. Mukharsky, C. Altimiras, H. le Sueur, P. Joyez, D. Vion, P. Roche, D. Esteve, J. Ankerhold, and F. Portier, *Physical Review Letters* **122**, 186804 (2019), publisher: American Physical Society.
- [13] A. Peugeot, G. Ménard, S. Dambach, M. Westig, B. Kubala, Y. Mukharsky, C. Altimiras, P. Joyez, D. Vion, P. Roche, D. Esteve, P. Milman, J. Leppäkangas, G. Johansson, M. Hofheinz, J. Ankerhold, and F. Portier, *Physical Review X* **11**, 031008 (2021), publisher: American Physical Society.
- [14] S.-l. Ma, X.-k. Li, Y.-l. Ren, J.-k. Xie, and F.-l. Li, *Physical Review Research* **3**, 043020 (2021), publisher: American Physical Society.
- [15] N. Lörch, C. Bruder, N. Brunner, and P. P. Hofer, *Quantum Science and Technology* **3**, 035014 (2018), publisher: IOP Publishing.
- [16] R. L. Kautz, *Reports on Progress in Physics* **59**, 935 (1996).
- [17] S. Shapiro, A. R. Janus, and S. Holly, *Reviews of Modern Physics* **36**, 223 (1964).
- [18] Likharev, *Dynamics of Josephson Junctions and Circuits* (CRC Press, 1986).

- [19] P. Richards, F. Auracher, and T. Van Duzer, *Proceedings of the IEEE* **61**, 36 (1973).
- [20] J. Zmuidzinas and P. Richards, *Proceedings of the IEEE* **92**, 1597 (2004), conference Name: Proceedings of the IEEE.
- [21] J. R. Tucker and M. J. Feldman, *Reviews of Modern Physics* **57**, 1055 (1985).
- [22] M. T. Levinsen, R. Y. Chiao, M. J. Feldman, and B. A. Tucker, *Applied Physics Letters* **31**, 776 (1977), _eprint: <https://doi.org/10.1063/1.89520>.
- [23] R. L. Kautz, *Applied Physics Letters* **36**, 386 (1980), _eprint: <https://doi.org/10.1063/1.91497>.
- [24] N. Beev and M. Kiviranta, *Review of Scientific Instruments* **83**, 066107 (2012).
- [25] I. Yanson, V. Svistunov, and I. Dmitrenko, *Sov. Phys. JETP* **21**, 650 (1965).
- [26] M. Hofheinz, F. Portier, Q. Baudouin, P. Joyez, D. Vion, P. Bertet, P. Roche, and D. Esteve, *Physical Review Letters* **106**, 217005 (2011).
- [27] M. C. Cassidy, A. Bruno, S. Rubbert, M. Irfan, J. Kammhuber, R. N. Schouten, A. R. Akhmerov, and L. P. Kouwenhoven, *Science* **355**, 939 (2017).
- [28] G.-L. Ingold and Y. V. Nazarov, Charge tunneling rates in ultrasmall junctions, in *Single Charge Tunneling: Coulomb Blockade Phenomena In Nanostructures* (Springer US, Boston, MA, 1992) Chap. 2, pp. 21–107.
- [29] T. Holst, D. Esteve, C. Urbina, and M. H. Devoret, *Phys. Rev. Lett.* **73**, 3455 (1994).
- [30] J. L. Stewart, *Proceedings of the IRE* **42**, 1539 (1954).
- [31] A. Peugeot, H. Riechert, S. Annabi, L. Balembois, M. Villiers, E. Flurin, J. Griesmar, E. Arrighi, J.-D. Pillet, and L. Bretheau, *Physical Review Applied* **22**, 064027 (2024).
- [32] R. Albert, J. Griesmar, F. Blanchet, U. Martel, N. Bourlet, and M. Hofheinz, *Physical Review X* **14**, 011011 (2024).
- [33] U. Martel, R. Albert, F. Blanchet, J. Griesmar, G. Ouellet, H. Therrien, N. Nehra, N. Bourlet, and M. Hofheinz, *Influence of bias voltage noise on the Inelastic Cooper-Pair Tunneling Amplifier (ICTA)* (2024), [arXiv:2409.18349](https://arxiv.org/abs/2409.18349).
- [34] T. Aissaoui, A. Murani, R. Lescanne, and A. Sarlette, *A cat qubit stabilization scheme using a voltage biased Josephson junction* (2024), [arXiv:2411.08132](https://arxiv.org/abs/2411.08132).